Puisto, A; Mohtaschemi, M; Alava, MJ; Illa, X

Dynamic hysteresis in the rheology of complex fluids

Published in:
Physical Review E

DOI:
10.1103/PhysRevE.91.042314

Published: 01/01/2015

Document Version
Publisher's PDF, also known as Version of record

Please cite the original version:
Puisto, A., Mohtaschemi, M., Alava, MJ., & Illa, X. (2015). Dynamic hysteresis in the rheology of complex fluids. Physical Review E, 91(4), 1-8. [042314]. https://doi.org/10.1103/PhysRevE.91.042314

Dynamic hysteresis in the rheology of complex fluids

Antti Puisto,* Mikael Mohtaschemi, and Mikko J. Alava
Department of Applied Physics, Aalto University, P.O. Box 11100, FI-00076 Aalto, Espoo, Finland

Xavier Illa
Departament d'Estructura i Constituents de la Matèria, Facultat de Fìsica, Universitat de Barcelona, Martí i Franquès 1, E-08028 Barcelona, Spain

(Received 11 March 2014; revised manuscript received 23 October 2014; published 27 April 2015)

Recently, rheological hysteresis has been studied systematically in a wide range of complex fluids combining global rheology and time-resolved velocimetry. In this paper we present an analysis of the roles of the three most fundamental mechanisms in simple-yield-stress fluids: structure dynamics, viscoelastic response, and spatial flow heterogeneities, i.e., time-dependent shear bands. Dynamical hysteresis simulations are done analogously to rheological ramp-up and -down experiments on a coupled model which incorporates viscoelasticity and time-dependent structure evolution. Based on experimental data, a coupling between hysteresis measured from the local velocity profiles and that measured from the global flow curve has been suggested. According to the present model, even if transient shear banding appears during the shear ramps, in typical narrow-gap devices, only a small part of the hysteretic response can be attributed to heterogeneous flow. This results in decoupling of the hysteresis measured from the local velocity profiles and the global flow curve, demonstrating that for an arbitrary time-dependent rheological response this proposed coupling can be very weak.

DOI: 10.1103/PhysRevE.91.042314 PACS number(s): 83.10.Rs, 47.57.Qk, 83.80.Hj

I. INTRODUCTION

Hysteresis is defined as a lag between the driving and the response signals of a nonlinear system. This behavior, a signature of nonequilibrium effects, is ubiquitous in nature, while the best-known example remains magnetism [1,2]. Athermal systems, which have a very complex free energy scenario with high energy barriers, only evolve under the application of an external field, manifested by rate-independent hysteresis. In systems with thermal behavior [3], hysteresis is rate dependent and due to competition between the driving and the relaxation rates.

In rheological systems hysteresis is associated with thixotropy, classically defined as the time-dependent reduction of viscosity under a constant shear rate [4]. Since recently even simple-yield-stress materials have turned out to show such relaxation, albeit at time scales shorter than the observation window [5], the division between thixotropic and simple fluids has become ambiguous. A more fundamental categorization considers the shapes of the fluids' intrinsic flow curves [6,7]. Simple-yield-stress fluids, showing only weak time dependence, also exhibit intrinsic flow curves of monotonic, Herschel-Bulkley shape, as opposed to strongly time-dependent ones, where the intrinsic flow curve has a nonmonotonic shape. As a consequence, only thixotropic fluids are expected to be prone to shear bands and the associated hysteretic behavior [8,9]. In this article, we discuss materials of a simple-yield-stress type.

Dynamical hysteresis appears in rheological experiments when the flow curve of the complex fluid is measured with a shear-rate or stress ramp [10,11]. The ramp usually consists of a series of discrete successive shear-rate or stress steps, each one associated with a certain waiting time, the time during which the shear rate is held constant. Depending on the waiting time, the number of shear-rate steps taken, and the material, the hysteresis loop is observed to have different shapes and areas [12–14]. The appearance of dynamical hysteresis in rheological data is classically taken as a sign of thixotropy. However, as recent experiments show, even nonthixotropic fluids show hysteresis. The reasons for this are still under debate, but based on experimental data there seems to be a link between hysteresis in the global rheology and transient shear banding [15].

Detailed experiments on rheological hysteresis and how it appears in *spatially resolved* velocimetry [16] were performed recently [15] for the first time. The experimental data were analyzed by computing the hysteresis loop areas from the data obtained from both the flow curves and, for some materials, also from the velocity profiles. Both hysteresis loop areas were found to depend on the waiting time by a "bell-shaped" relation in the case of classic thixotropic fluids [15]. This means that hysteresis vanishes at short and long waiting times and shows a maximum at intermediate times, in analogy to magnetic systems [2]. The generic behavior is reasoned to follow from two limits: When the applied waiting time is much shorter than a material-specific characteristic time scale, the structure changes are small, and the hysteresis is strongly decreased. On the other hand, if the waiting time is much longer than the characteristic time scale, the response is at steady state, showing no hysteresis. Intermediate waiting times lead to a maximum and a bell-shaped hysteresis curve. Time scales obtained from both the spatial velocity profiles and the flow curve gave rise to a single time scale for some low-density-yield-stress fluids. Based on this and the fact that, with one exception, the other materials showed similar hysteresis in the flow curve, the authors further hypothesize that this might be a universal behavior in a broad class of complex fluids, for which they find a bell-shaped hysteresis area of the flow curves. For simple-yield-stress materials, only the decreasing part of this

*antti.puisto@aalto.fi

relation was experimentally reachable. This was speculated to be due to the fast structure evolution dynamics, beyond the limit of experimentally accessible waiting times.

Rheological hysteresis has been observed before in complex fluid models under shear rheology [17] in connection with boundary conditions [18], and oscillatory rheology [19,20] as well as during transients between two rheological states [21]. The purpose of the present article is to analyze the proposed universality of the relation between the flow heterogeneities and flow curve hysteresis in complex fluids: Do the two methods universally measure a single material characteristic time scale, or can the time-dependent rheological response of the material have a functional form where this relation between the velocity profiles and the flow curve hysteresis does not hold? To do this, we perform numerical simulations utilizing a model introduced earlier, which captures qualitatively the dynamics of fluidization of a simple-yield-stress fluid [22]. We compute the shear-rheology-related hysteresis under both homogeneous shear and concentric-cylinder Couette flows: Their difference resolves the role of the fluid internal dynamics that couples the structure with the local viscosity, viscoelastic response due to internal structure, and time-dependent shear bands. We show that in our simple example the time scales obtained from velocity profiles and flow curves are indeed decoupled, hinting that the correlated time scales, experimentally observed in a laponite suspension, are a special case. Furthermore, we argue that hysteresis in rheological experiments is not based on a simple material time scale but, rather, on a spectrum of time scales imposed by the experimental protocol due to the shear-rate dependence of the material rheological response. We demonstrate that the typical bell-shaped relation between the dynamical hysteresis area and the waiting time can change to a more complicated scenario in strongly viscoelastic materials. This can be induced by additional relaxation time scales, e.g., due to structural elasticity. The rest of the paper is divided into three sections: Model (Sec. II), Results (Sec. III), and Conclusions (Sec. IV). Section II introduces the reader to the models and methods applied. In Sec. III the model is analyzed and results are presented from the perspective of recent related experimental studies. Finally, Sec. IV summarizes the main findings.

II. MODEL

Aggregating colloidal suspensions and microgels share the property of jamming liquid inside solid-like structures. In the first case the structure is formed of particle networks [23,24], and in the second case, of elastic sponge-like elements [25]. Thus, here we take the natural way of modeling the structure evolution through that of the immobilized portion of the volume. An example of a model utilizing these ideas is the one studied in Ref. [22]. There the approach was previously observed to qualitatively capture features of the fluidization of a simple-yield-stress fluid [22]. Under simple shear flow characterized by the shear rate, $\dot{\gamma}$, the time evolution of the jammed volume fraction, later called the *structure dynamics*, may be described by

$$\frac{d\phi}{dt} = \frac{A_b}{(\eta/\eta_o)^m} + (A_s - B_s\phi)\left(\frac{|\dot{\gamma}|}{\dot{\gamma}_0}\right)^k, \tag{1}$$

which contains terms for shear-independent (A_b, η_0, m) and shear-dependent growth and breakage (A_s, B_s, and k) of ϕ. k and $\dot{\gamma}_0$ (set to unity) both relate to the volume-fraction sensitivity to shearing. A_b, η_0, and m describe the growth of ϕ due to shear-independent recovery mechanisms. The viscosity of such a system diverges as the volume fraction approaches the maximum packing fraction ϕ_m, captured by a Krieger-Dougherty type of equation, $\eta(\phi) = \eta_0(1 - \frac{\phi}{\phi_m})^{-\kappa}$, which takes into account the "softness" of the jammed elements, κ, and the solvent viscosity η_0.

In the simplest scenario the stress is viscous, i.e., $\sigma = \dot{\gamma}\eta$. More complex constitutive equations take into account the stress or strain history, such as the Maxwell and Kelvin-Voigt models [26]. Since we consider the flowing state, the Maxwell stress model,

$$\sigma = \dot{\gamma}\eta + \frac{\eta}{G_0}\dot{\sigma}, \tag{2}$$

is applied for comparison, in addition to the Newtonian stress model. Here, the elastic stress is controlled by G_0, the continuum scale elastic modulus of the fluid. Up to this point the models allow no spatial heterogeneity, and we refer to them, being equivalent to a planar Couette scenario, as the *homogeneous viscous* and *homogeneous viscoelastic shear models*, respectively.

As can be observed in Eq. (1), there is no unique time scale associated with the relaxation of ϕ. Instead this depends on the shear rate and the initial condition ϕ_0. In other words, unless the fluid is in the steady state, it obtains the steady state at a rate which depends on the applied shear rate and its shear history. Furthermore, since the growth (A_b, A_s) and breakage (B_s) rates are not equal the relaxation rate is asymmetric around the steady state even at the same shear rate: The time scale depends on whether the ϕ is increasing or decreasing. With these properties, the model follows first-principles colloidal models, in which the kernels are usually asymmetric and shear dependent [9,27,28], and complies with what is found experimenally as well [29–33]. Finally, the Maxwell stress element in the viscoelastic model introduces another time scale through stress evolution, which can be tuned using G_0.

A spatial degree of freedom is required to allow for shear bands, observed to emerge during rheological experiments [15,29]. Integrating the radial component of the momentum equation in cylindrical coordinates we obtain an expression for the tangential stress,

$$\sigma = \frac{C}{r^2}, \tag{3}$$

where C is the integration constant. Substituting Eq. (3) into Eq. (2) it is easy to write the expression for the shear rate,

$$\dot{\gamma}(r) = \frac{C}{r^2\eta(r)} - \frac{1}{G_0 r^2}\frac{dC}{dt}. \tag{4}$$

To obtain C we impose no-slip boundary conditions and solve this differential equation, where the initial value $C(t = 0)$ takes into account the elastic residual stress of the fluid. Due to the simulation procedure, which includes a preshear period, it makes sense to set this value to $C(t = 0) = 0$.

The shear rate as a function of the radial position in the viscous case ($G \to \infty$) reads [34]

$$\dot{\gamma}(r) = \frac{\Omega_b - \Omega_a}{\eta(r) r^2 \left[\int_{R_a}^{R_b} \frac{1}{r^3 \eta(r)} dr \right]}, \tag{5}$$

where Ω_a (Ω_b) and R_a (R_b) are the angular velocity and radius of the inner (outer) cylinder, respectively, and $\eta(r)$ is the local viscosity. The viscoelastic case requires numerical solution. The above approximations neglect the influence of wall slip, found to have a minor effect on hysteresis in experiments [15]. Here, unless specified otherwise, we set the device dimensions to $R_a = 24.0$ mm and $R_b = 25.0$ mm, resulting in a gap size $\delta = 1.0$ mm, typical values used in such experiments [15]. The implementation involves a separate structural model at 400 radial positions, computing new estimates for the local shear rate during each integration step. Although with the present approximation, rotating each of the cylinders will produce an equivalent stress profile, in the following the inner cylinder is given an angular velocity based on the apparent shear rate [35]:

$$\dot{\gamma}_a = (\Omega_b - \Omega_a) \frac{2R_b^2}{R_b^2 - R_a^2}. \tag{6}$$

In what follows the models implementing concentriccylinder geometry are called the *heterogeneous viscous* and *viscoelastic shear models*. The practical implementation is a C++ program, utilizing the CVODE routines of the SUNDIALS libraries for the time integration [36].

The steady-state flow curve, independent of the stress model used [37], can be used to fix the ratios of A_s, A_b, and B_s. Their absolute values are related to the structure dynamics time scales. The model parameters are chosen such that the steady-state stress values in the range $\dot{\gamma}_a = 1.0\,\mathrm{s}^{-1}$ and $\dot{\gamma}_a = 1000\,\mathrm{s}^{-1}$ roughly follow experimental rheological characteristics of a typical simple-yield-stress fluid [15]. The model does not allow for quantitative fitting since it gives a Herschel-Bulkley ($\sigma = \sigma_0 + A\dot{\gamma}^{\alpha}$) exponent $\alpha = 1$, whereas in the experiments the exponent is typically somewhat smaller. The parameters of the kinetic equation utilized in the following analysis are $A_s = 0.01$, $B_s = 0.0157$, $A_b = 1.051$. In order to reproduce typical fluidization dynamics of a simple-yield-stress fluid we set $k = 2$ and $m = k$ to have a simple-yield-stress flow curve [22]. Finally, for the constitutive equation we use a compatible set of parameters: $\eta_0 = 0.001$ Pa s, $\phi_m = 0.68$, and $\kappa = 2.2$. We have checked that the qualitative model behavior is not influenced by these selections. In addition, in the viscoelastic stress model the elastic modulus G_0 is a free parameter, and its influence is analyzed later.

III. RESULTS

The simulations here follow the usual experimental protocol [15], where, after a long-lasting preshear period at the highest shear rate, one sweeps the shear rate first down and then back up. The preshear period in simulations is performed at $1000\,\mathrm{s}^{-1}$ until steady state is reached. This is the initial condition for Eq. (1). This is a common approach in rheological characterization of thixotropic materials [4,12,15]. Using the viscous stress model and applying the homogeneous and heterogeneous shear models, we arrive at the flow curves plotted at different waiting times shown in Fig. 1. As shown in the figure, waiting-time-dependent hysteresis appears in the flow curves at low shear rates under both homogeneous (left column) and heterogeneous (right column) shear. Interestingly, despite the fact that the homogeneous shear model ignores spatial effects, the flow curves of the two shear models look almost the same. This shows that hysteresis is simply a result of the interplay between the structure dynamics, which is proportional to $\dot{\gamma}^{-k}$, and the constant waiting time applied in the shear-rate ramps, independent of the possible flow heterogeneities allowed by the concentric-cylinder geometry.

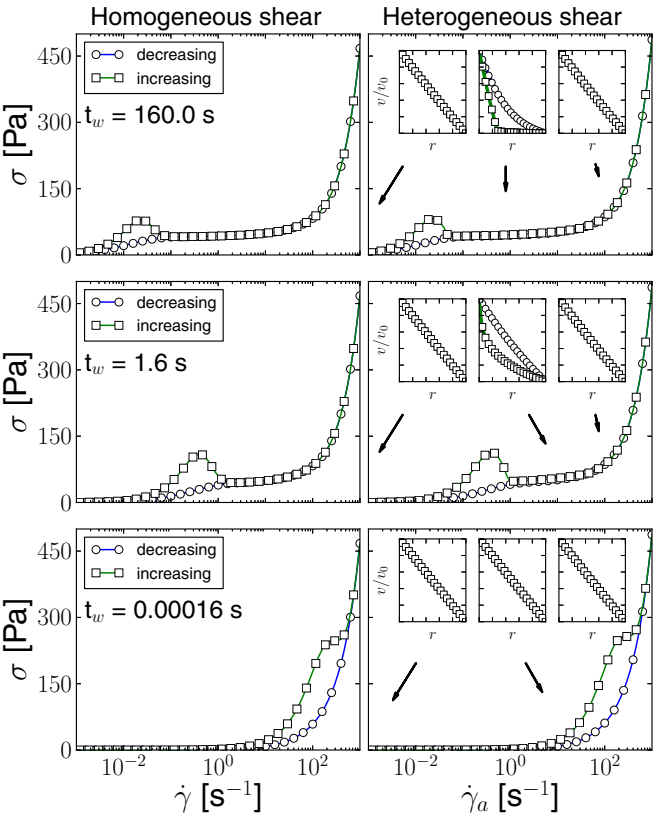

FIG. 1. (Color online) Flow curves, stress σ versus shear rate $\dot{\gamma}$, and stress versus average shear rate $\dot{\gamma}_a$, computed using the homogeneous and heterogeneous models, respectively. Decreasing and increasing ramps are simulated for different waiting times t_w, taking into account only the viscous stress. Insets: Velocity profiles during simulations at shear rates of $0.001\,\mathrm{s}^{-1}$ (left), $1.0\,\mathrm{s}^{-1}$ (center), and $100.0\,\mathrm{s}^{-1}$ (right). Short waiting times result in linear velocity profiles during both ramps, while longer waiting times give shear-banded profiles during the increasing-shear-rate ramp.

Furthermore, when the waiting time is short compared to the applied shear rate, the measured flow curves deviate from the steady-state one. At this point the measured flow curve falls below the steady state during the decreasing ramp. During the upwards ramp, the measured flow curve eventually goes above the steady state after a certain point. Finally, as is often the case in experiments, in simulations the decreasing and increasing flow curves at high shear rates exactly match. At low shear rates, a maximum $[\max(\sigma_{\mathrm{increasing}}(\dot{\gamma}) - \sigma_{\mathrm{decreasing}}(\dot{\gamma})]$ in the flow curve hysteresis is seen. The shear rate at which this maximum occurs depends on the applied waiting time.

Furthermore, the stress at low shear rates (dynamic yield stress) approaches 0 when the waiting time is much below the dynamical structure growth time associated with the lowest measured shear rate.

Allowing for spatial heterogeneity in the shear-rate results in transient shear banding familiar in startup flows [22,29]. Here, transient shear bands occur during the increasing-shear-rate ramp (shown in the insets in Fig. 1), in agreement with recent experiments [15]. In the simulated flow curves it appears as a long tail, which is somewhat difficult to distinguish, after the local stress maximum during the increasing ramp. The duration of this regime depends on the waiting time. With longer waiting times, the system is more jammed when the increasing-shear-rate ramp begins, thus leading to longer fluidization times (more persistent transient shear bands). In fact, the transient shear-banding regime vanishes altogether at sufficiently short waiting times leading to homogeneous relaxation. Despite this, the structure dynamics persists for a while, as shown in the lowest panel in Fig. 1.

The interpretation of the flow curves is simplified when one considers viscosity evolution in the homogeneous shear case, which reflects directly the evolution of ϕ. This is plotted with different waiting times, along with the corresponding steady state (black line), in Fig. 2. Decreasing the waiting time drops the measured viscosity further and further below the steady state. Moreover, as is obvious judging by Eq. (1), the structure dynamics gets slower with decreasing shear rate, which tends to increase the effect at low shear rates. In the decreasing-shear-rate ramp the viscosity always remains below the steady state. During the increasing-shear-rate ramp the viscosity first starts to approach the steady state value from below, crosses it at some waiting-time-dependent point, and, due to the slow relaxation, finally ends up approaching the steady-state line from above. Thus, the fact that this relaxation is shear rate dependent, an experimentally known fact, already implies an asymmetry between the increasing and the decreasing shear rate sweeps, resulting in hysteresis. Indeed, it can be noted that

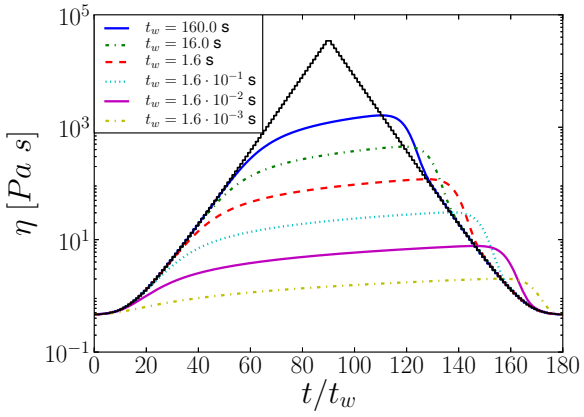

FIG. 2. (Color online) Time evolution of the fluid viscosity η during the hysteresis cycle at different waiting times t_w. The black line represents the steady state. At shorter waiting times, the viscosity falls from the steady-state line sooner. The hysteresis is a result of the asymmetry between the relaxation pattern with decreasing and that with increasing shear rates, i.e., around the centerline here located at $t/t_w = 90$.

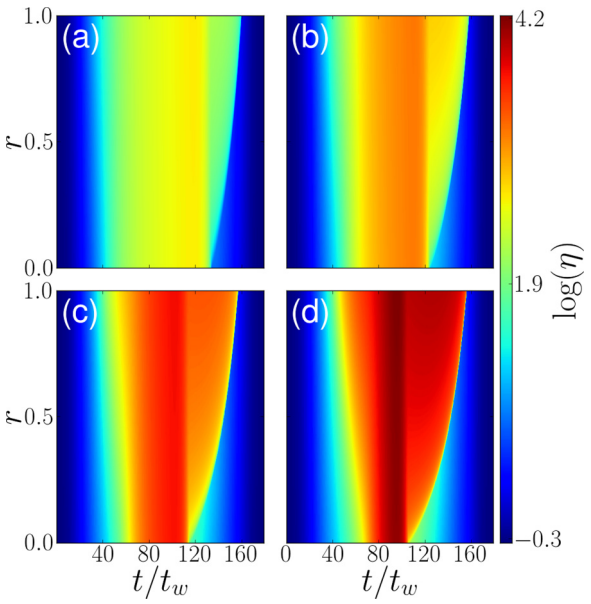

FIG. 3. (Color online) Time evolution of the fluid viscosity η over the gap during the hysteresis cycle at different waiting times t_w in the heterogeneous shear model. A clear shear-banded region is seen during the increasing-shear-rate ramp (starting at $t/t_w = 90$) independent of the waiting time. Waiting times are (a) s, (b) 16 s, (c) 160 s, and (d) 1600 s. The color bar runs from the fluidized state (dark blue) to the high-viscosity state (dark red).

the only cases symmetric around the centerline (i.e., lowest shear rate) which would not produce hysteresis in the flow curves are the ones where the fluid does not have time to respond to the external drive ($t_w \to 0$) and the steady state.

Next we discuss the spatiotemporal maps of the local viscosity in the heterogeneous shear model plotted in Fig. 3. They show the evolution of the local viscosity (color-coded) at each position (vertical axis) as a function of time (horizontal axis). The overall picture follows the homogeneous one; the plots are asymmetric around the centerline. In addition, each of the plots shows strong spatial variation of the viscosity inside the concentric-cylinder gap, especially during the increasing-shear-rate ramp. Right after the increasing-shear-rate ramp starts, a splitting of the fluid into low- and high-viscosity bands is seen. The low-viscosity band increases throughout the increasing-shear-rate ramp, in time spreading over the whole gap. At shorter waiting times, the spatial effect is less pronounced due to the fact that the maximum viscosity reached is inversely proportional to the waiting time. This, on the other hand, decreases the contrast between the two shear bands.

The computed flow curves using the viscoelastic stress model are plotted as an example for the $G = 64.0$ case in Fig. 4. The viscoelastic stress model only slightly modifies these at long waiting times, irrespective of the applied geometry. The transient shear-banding regime at long waiting times also remains virtually untouched. At short waiting times, however, the stress derivative corresponding to elastic deformations gets large and results in a significant difference in both the flow curves and the velocity profiles. Here, typical startup effects such as backward recoil flows appear before the system is returned to the linear velocity profile. This is expected for a

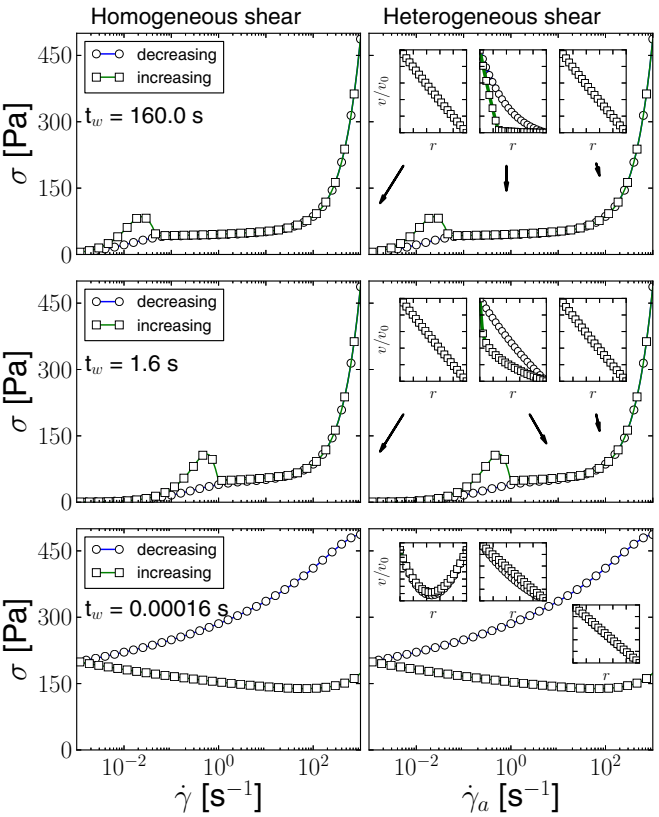

FIG. 4. (Color online) Flow curves computed with subsequent decreasing- and increasing-shear-rate ramps for different waiting times t_w, taking into account the viscoelastic stress. Insets: Velocity profiles during simulations at shear rates 0.001 s^{-1} (left), 1.0 s^{-1} (center), and 100.0 s^{-1} (right). Viscoelastic effects appear only when the shortest waiting times are applied. Longer waiting times give essentially the same response as in the viscous case.

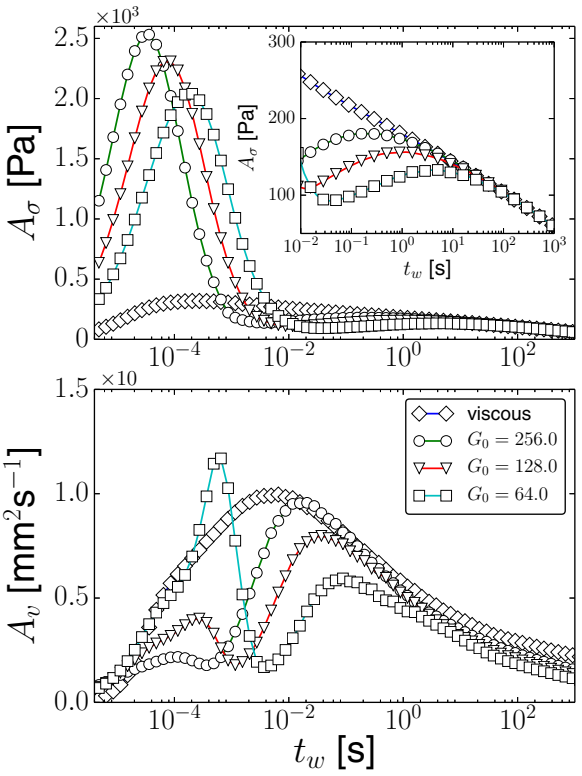

FIG. 5. (Color online) Hysteresis loop areas computed from the flow curve A_σ (top) and velocity profiles A_v (bottom) plotted on a semilogarithmic scale for the viscous stress model and the viscoelastic stress model with different elastic moduli G_0. Hysteresis loop areas decrease with decreasing G_0. Inset: Zoom of A_σ close to the experimental range.

viscoelastic system [4]. At short waiting times the systems behavior resembles much the oscillatory experiments: At the lowest waiting time the deformations are so small that a real system would remain in the linearly viscoelastic regime. Interestingly, the hysteresis loop is open at the lowest waiting times and, therefore, seems to escape from the observation window.

Reference [15] proposes analyzing the hysteresis with the help of

$$A_\sigma = \int_{\dot{\gamma}_{\min}}^{\dot{\gamma}_{\max}} |\Delta\sigma| d(\log\dot{\gamma}) \tag{7}$$

for the hysteresis area between the two flow curves and

$$A_v = \int_{\dot{\gamma}_{\min}}^{\dot{\gamma}_{\max}} \int_{R_a}^{R_b} |\Delta v| dr d(\log\dot{\gamma}) \tag{8}$$

for the hysteresis areas computed from the velocity profiles. These definitions logarithmically weight hysteresis areas, i.e., give more importance to the low-shear-rate end. As discussed earlier, these measure the symmetry of the dynamics between the growth and the destruction of the structure and should not be considered a measure of the distance from the steady state. The hysteresis loop areas A_σ and A_v computed for these results are plotted in Fig. 5. In the viscous case they increase monotonically with decreasing waiting times in the experimentally accessible waiting time range (around 1.0–1000.0 s). This occurs even for the A_v, despite the fact that the velocity profiles seemingly get more heterogeneous during the increasing-shear-rate ramp. The reason is that at long waiting times also during the decreasing ramp some shear localization occurs, as can be seen in the velocity profiles in Fig. 1. Below this waiting-time range, the hysteresis areas reach a maximum (A_σ at around $t_w = 0.001$ s and A_v a decade later). At even shorter waiting times, the hysteresis areas start decreasing again. The absolute values of the waiting times at which the transitions occur relate to the kernels in Eq. (1) and, thus, can be changed to arbitrary values by rescaling the kernels without affecting the qualitative behavior.

The viscoelastic stress model changes the picture at short waiting times by an additional time scale (τ_σ), which introduces a second maximum. The location of this second maximum for both A_σ and A_v, depends on the elastic modulus, as shown in Fig. 5. The inset in the top panel in Fig. 5 shows A_σ as a function of t_w near the hysteresis maxima of the viscoelastic model. As shown in the figure, the bell shape of the hysteresis loop areas can be the result of one of two mechanisms: either due to the viscous response at waiting times around the hysteresis maximum or due to the viscoelastic response with the observation window around

the second maximum (for the lowest G_0 in the inset in Fig. 5). Double-peaked hysteresis loop areas have not been seen experimentally and might appear only in materials having a long structure dynamics time scale and a low elastic modulus, such as microfibrillated cellulose suspensions [12]. In the very short waiting time range the simulations approach the oscillatory shear measurements, which are commonly used to probe the viscoelastic properties of soft materials. The shapes of A_σ and A_v look similar, in agreement with Ref. [15]; in contrast, with the present parameters the simulated maxima of the two hysteresis curves are located at different waiting times. In extensive tests this behavior was found to depend on the values of k, m, and G_0. For instance, in the case $k = m = 1$, both maxima approximately overlap. This indicates that the two properties are decoupled in the general case but might be coupled for some special time-dependent rheological responses. Thus, further experimental work is required to understand the (de)coupling between A_σ and A_v in different types of soft glassy materials.

A larger gap width gives more importance to the spatial flow heterogeneity. This occurs since the distance the shear-band edge travels to reach the stator during the increasing-shear-rate ramp becomes larger and the edge velocity is proportional to the (imposed) average shear rate, as mentioned in Ref. [22]. To demonstrate this, we have plotted the flow curve for the viscous, heterogeneous shear case, using a gap size of 10 mm and $t_w = 160$ s in Fig. 6. A comparison of it to the ones computed using a narrower gap size demonstrates that the transient shear-banding regime extends into higher shear rates during the upward ramp.

To see whether the gap width influences the correlation between the two hysteresis maxima, we computed the hysteresis loop areas for three gap widths for the viscous, heterogeneous shear case plotted in Fig. 7. Increasing the gap makes the shear-banded flows more permanent, requiring much longer waiting times for the hysteresis to vanish. Because of this, the maxima of the two curves approach one another. The amplitude of the hysteresis loop areas, computed both from the flow curve and from the velocity profiles, increases.

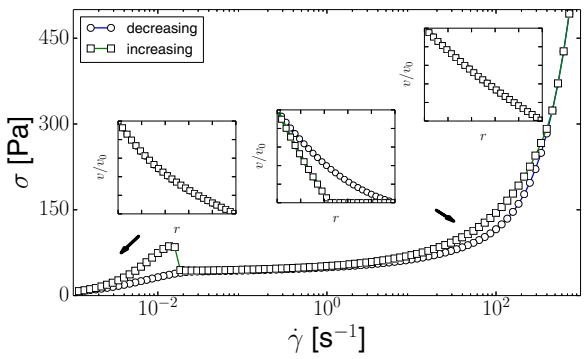

FIG. 6. (Color online) Example of a flow curve computed with the gap width $\delta = 10$ mm and $t_w = 160$ s. Insets: The hysteresis is more pronounced at intermediate shear rates due to the increased flow heterogeneity as shown in these velocity profiles; shear rates corresponding to the velocity profiles are 0.001 s^{-1} (left), 100.0 s^{-1} (center), and 540 s^{-1} (right).

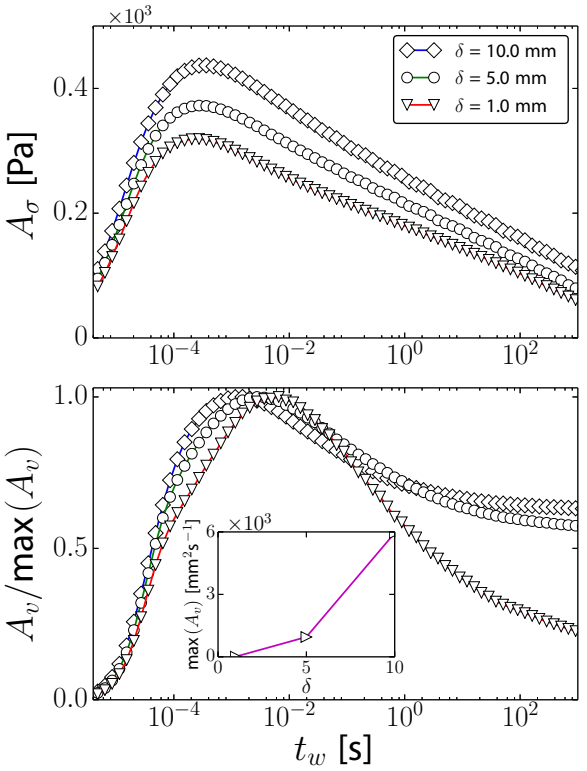

FIG. 7. (Color online) Hysteresis loop areas A_σ and A_v compared for different gaps δ.

IV. CONCLUSIONS

We have studied the origin of the rheological hysteresis loop through a structural kinetics model of a simple time-dependent yield stress fluid. In the model, the structure dynamics is proportional to $\dot{\gamma}^{-k}$, a known fact in some of the first-principles collision models for colloids [9,27,28] and also experimentally observed in numerous complex fluids [29–33]. Since the fluid structure dynamically relaxes at a rate imposed by the current shear rate, but the waiting time t_w in the experimental protocol is fixed, below a certain shear rate, the structure fails to recover the steady state. Thus, such an experiment is a convolution of series of relaxation times each associated with a different shear rate and the initial condition set by the fluid's history.

The two directions of the shear-rate ramp differ. In the decreasing ramp the structure is growing and the stress therefore falls below the steady-state value. In the increasing-shear-rate ramp, the structure is initially growing. At some point it passes through the steady-state structure, after which it starts to break again. From this point on, the stress is always above the steady-state value, until, owing to the increasing shear rate, the structural dynamics again reaches steady state before the end of the waiting time. Therefore, the high-shear-rate parts of the two flow curves are the same.

Despite its shortcomings, the model used here recovers some of the delicate features of the experiments such as the flow heterogeneity in startup flows [22]. Here, in agreement with observations in Ref. [15], these transient shear bands appear during the increasing-shear-rate ramp. This allowed us to analyze the role of these flow heterogeneities in the

reported flow curve. To do this, we computed the homogeneous shear case, where the local shear rate was imposed, and the concentric-cylinder Couette, where the angular velocity of the inner cylinder was adjusted to set a global shear rate over the gap. Comparison of the two made it possible to observe that only a negligible portion of the flow curve hysteresis was due to the flow heterogeneities. This already implied a decoupling of the flow heterogeneities and the flow curve in a narrow-gap device. Increasing the gap width was found to increase the relative importance of the flow heterogeneities to the global flow curve and, therefore, lead to enchanced coupling between A_σ and A_v.

Furthermore, we computed the hysteresis loop areas, as proposed based on the experiments [15]. In agreement with experimental observations we found "bell-shaped" curves with the viscous stress model for both A_σ and A_v. With the present set of parameters and the present rheological model, the maxima of the two hysteresis loop areas appeared at different waiting times, in contrast to what was reported for a thixotropic laponite suspension in Ref. [15]. Thus, we conclude that such coupling between the two quantities is a specific property of the time-dependent rheological response of the particular complex fluid (type). Our results show that universality of the coupling among all soft glassy materials would imply similarity of their rheological responses. Given that the physical origin of the structure dynamics varies among classes of soft glassy materials, such universality of their rheological responses can be deemed highly improbable. However, this property would enable the development of a universal model of soft glassy materials. To elaborate on this point, more experimental evidence is required to probe the relation of A_σ and A_v among a larger portion of soft glassy materials.

The model implements only simple no-slip conditions at solid-liquid boundaries. This could be justified, since experiments show no significant difference in the hysteresis due to different surface roughnesses [15]. However, despite rough surfaces, the experiments report significant slip at the solid-liquid boundaries. Thus, we suspect that this effect could be significant, especially at low shear rates. Such an effect would be expected to confer more importance to the heterogeneous flow (reducing the hysteresis loop at low shear rates) when A_σ is computed, i.e., it would make A_σ and A_v more correlated. Thus far, there exist no good alternatives for such boundary conditions. Finding the proper ones for particular types of yield stress materials remains a subject for future research.

ACKNOWLEDGMENTS

We thank T. Divoux and S. Manneville for fruitful discussions. This work was supported by the Effnet program of the Finnish Forest Cluster Ltd. and the EU framework 7 program SUNPAP. Also, support from the Academy of Finland through the Project Nos. 251748 (COMP Center of Excellence Programme), 140268, 278367, and within the framework of the International Doctoral Programme in Bioproducts Technology (PaPSaT) is acknowledged. X.I. acknowledges the financial support from Programa Juan de la Cierva and Project MAT2013-40590-P.

[1] G. Bertotti, *Hysteresis in Magnetism: For Physicists, Materials Scientists and Engineers* (Academic Press, New York, 1998).
[2] B. K. Chakrabarti and M. Acharyya, Rev. Mod. Phys. **71**, 847 (1999).
[3] G. Bertotti and I. Mayergoyz, *The Science of Hysteresis* (Academic Press, New York, 2006).
[4] J. Mewis and N. Wagner, Adv. Colloid Interfac. **147**, 214 (2009).
[5] P. Coussot and G. Ovarlez, Eur. Phys. J. E **33**, 183 (2010).
[6] P. C. F. Møller, A. Fall, V. Chikkadi, D. Derks, and D. Bonn, Philos. T. Roy. Soc. A **367**, 5139 (2009).
[7] P. Coussot, Q. D. Nguyen, H. T. Huynh, and D. Bonn, Phys. Rev. Lett. **88**, 175501 (2002).
[8] G. Ovarlez, S. Rodts, X. Chateau, and P. Coussot, Rheol. Acta **48**, 831 (2009).
[9] M. Mohtaschemi, A. Puisto, X. Illa, and M. J. Alava, Soft Matter **10**, 2971 (2014).
[10] L. B. Chen, C. F. Zukoski, B. J. Ackerson, H. J. M. Hanley, G. C. Straty, J. Barker, and C. J. Glinka, Phys. Rev. Lett. **69**, 688 (1992).
[11] T. Divoux, C. Barentin, and S. Manneville, Soft Matter **7**, 8409 (2011).
[12] M. Iotti, Ø. W. Gregersen, S. Moe, and M. Lenes, J. Polym. Env. **19**, 137 (2010).
[13] J. Labanda and J. Llorens, J. Colloid Interf. Sci. **289**, 86 (2005).
[14] A. Papo and L. Piani, Cement Concrete Res. **34**, 2097 (2004).
[15] T. Divoux, V. Grenard, and S. Manneville, Phys. Rev. Lett. **110**, 018304 (2013).
[16] S. Manneville, Rheol. Acta **47**, 301 (2008).
[17] J. Labanda and J. Llorens, Rheol. Acta **45**, 305 (2006).
[18] J. Adams, S. Fielding, and P. Olmsted, J. Non-Newton. Fluid Mech. **151**, 101 (2008).
[19] P. Sollich, Phys. Rev. E **58**, 738 (1998).
[20] J. J. Stickel, J. S. Knutsen, and M. W. Liberatore, J. Rheol. **57**, 1569 (2013).
[21] A. Visintin, Rend. Semin. Mat. Univ. Padova **77**, 213 (1987).
[22] X. Illa, A. Puisto, A. Lehtinen, M. Mohtaschemi, and M. J. Alava, Phys. Rev. E **87**, 022307 (2013).
[23] P. L. Krapivsky, S. Redner, and E. Ben-Naim, *A Kinetic View of Statistical Physics* (Cambridge University Press, Cambridge, UK, 2010).
[24] A. R. Heath, P. A. Bahri, P. D. Fawell, and J. B. Farrow, AIChE J. **52**, 1641 (2006).
[25] J. Piau, J. Non-Newton. Fluid Mech. **144**, 1 (2007).
[26] W. M. Lai, D. Rubin, and E. Krempl, *Introduction to Continuum Mechanics*, 3rd. ed. (Elsevier, Amsterdam, 1993).
[27] M. Vanni and G. Baldi, Adv. Colloid Interf. Sci. **97**, 151 (2002).
[28] M. U. Bäbler, AIChE J. **54**, 1748 (2008).
[29] T. Divoux, D. Tamarii, C. Barentin, and S. Manneville, Phys. Rev. Lett. **104**, 208301 (2010).
[30] B. M. Erwin, D. Vlassopoulos, and M. Cloitre, J. Rheol. **54**, 915 (2010).

[31] M. Siebenbürger, M. Ballauff, and T. Voigtmann, Phys. Rev. Lett. **108**, 255701 (2012).
[32] J. D. Martin and Y. T. Hu, Soft Matter **8**, 6940 (2012).
[33] L. Bécu, P. Grondin, A. Colin, and S. Manneville, Colloids Surf A: Physicochem. Eng. Aspects **263**, 146 (2004).
[34] R. J. Phillips, R. C. Armstrong, R. A. Brown, A. L. Graham, and J. R. Abbott, Phys. Fluids A **4**, 30 (1992).
[35] T. G. Mezger, *The Rheology Handbook: For Users of Rotational and Oscillatory Rheometers* (Vincentz Network, Hannover, Germany, 2006).
[36] S. D. Cohen and A. C. Hindmarsh, Comp. Phys. **10**, 138 (1996).
[37] A. Lehtinen, A. Puisto, X. Illa, M. Mohtaschemi, and M. J. Alava, Soft Matter **9**, 8041 (2013).